No-Pair Bonding in the High-Spin $^3\Sigma_u^+$ State of Li_2. A Valence Bond Study of Its Origins

David Danovich,† Wei Wu,†,‡ and Sason Shaik*,†

Contribution from the Department of Organic Chemistry and the Lise Meitner-Minerva Center for Computational Quantum Chemistry, The Hebrew University, 91904 Jerusalem, Israel

Received August 13, 1998. Revised Manuscript Received January 21, 1999

Abstract: Lithium forms high-spin clusters, $^{n+1}Li_n$ which are bonded even though there are no electron-pairs! This no-pair bonding is weak for the $^3\Sigma_u^+$ state of Li_2 but becomes very significant for larger clusters reaching up to 1.8 eV for $^7Li_6$. To understand the nature of "no-pair bonding", we performed valence bond (VB) calculations on the states of Li_2, benchmarked them against high-level MO-based calculations which account for static as well as dynamic electron correlation, and derived bonding mechanisms for the no-pair triplet state *vis a vis* the singlet ground state. It is shown that both the singlet-pair and no-pair bonds are bonded by covalency but differ in the mechanism of VB mixing. The singlet-pair bond is sustained by covalency augmented by Coulomb correlation of the electron pair, while the no-pair bond originates solely in the resonance energy between the repulsive fundamental triplet VB structure with the secondary VB structures. Understanding of the fundamental no-pair bond in $^3Li_2$ enables one to derive insight into the bonding and geometric features of no-pair $^{n+1}Li_n$ high-spin clusters. Experimental characterization of such clusters will broaden the current conception of bonding beyond the traditional spin-pairing paradigm.

1. Introduction

According to both molecular orbital (MO) and valence bond (VB) theories, singlet electron-pairing is a fundamental form of bonding in the ground state of molecules, whereas triplet-pairing is associated with a repulsive antibonding interaction.[1] Using the H_2 molecule as an archetypal species that subscribes to this paradigm, one knows that the ground state which exhibits spin-pairing is bonded while the first triplet excited state, $^3\Sigma_u^+$, which is devoid of spin-pairing is repulsive throughout[2,3] and unbound. This paradigm seems, however, to break down as we move away from H_2 to bonding in alkali dimers and higher clusters. Thus, in contrast with the triplet $^3\Sigma_u^+$ state of H_2, the same state of Li_2 is bound, albeit by a small amount.[4−9] This property of Li_2, first pointed out by Kutzelnigg et al.[4] and then by Olson and Konowalow,[5] has been highlighted in a recent paper by Glukhovtsev and Schleyer,[9] who have shown that high-spin $^{n+1}Li_n$ clusters exhibit bonding which becomes substantial and scales with the size of the cluster (reaching 1.48 eV for $^7Li_6$), despite the lack of any electron pairs between the atoms. Glukhovtsev and Schleyer[9] have called this bonding type *"no-pair bonding"* and noted that all the no-pair bonded species appear in highly symmetric geometries which *are unstable for low-spin situations*. Table 1 shows the results of Glukhovtsev and Schleyer[9] along with our test results performed at a higher level of geometry optimization and correlation treatment. It is apparent that no-pair bondings along with the symmetric geometries of the respective species are reproduced at the higher level and that no-pair bonding can sustain sizable magnetic clusters with substantial bonding energy. This and the fact that the $^3\Sigma_u^+$ state of Cs_2 has been recently characterized by photo-

Table 1. No-Pair Bond Energies (eV) for $^{n+1}Li_n$ and $^{n+1}Na_n$ Clusters

entry	Li_n	sym	state	D_e[a]	D_e[b,d]	Na_n	D_e[c,d]
1	Li_2	$D_{\infty h}$	$^3\Sigma_u^+$	0.027	0.032	Na_2	0.018
2	Li_3	D_{3h}	$^4A_1$	0.341	0.442	Na_3	0.085
3	Li_4	T_d	$^5A_1$	1.099	1.282	Na_4	0.321
4	Li_5	C_{4v}	$^6B_1$	1.277	1.537		
5	Li_6	$D_{4h}(O_h)$[e]	$^7A_{2u}$ ($^7T_{1u}$)	1.477	1.846		

[a] Calculated at the UQCISD(T,fc)/6-31G*//UMP2(full)/6-31G* level of theory. The letter "U" stands for "unrestricted" procedure (different orbitals for different spins). The disignator "fc" means that the correlation calculation does not include core electrons. Data from ref 9. [b] Calculated at the UCCSD(T,full)/cc-pVDZ level of theory. [c] Calculated at the UCCSD(T,full)/cc-pVDZ level of theory. [d] This work. [e] The molecule is virtually O_h with Li−Li distances 3.1252 Å (the "axial" bonds) and 3.1216 Å (the basal bonds). The energy of the O_h (Li−Li distances are 3.1247 Å) and D_{4h} structures is the same.

* To whom correspondence should be addressed. E-mail: sason@yfaat.ch.huji.ac.il.

† Hebrew University.

‡ Permanent address: Department of Chemistry, Xiamen University, Xiamen, Fujian 361005, P. R. of China.

(1) See for example: Pilar, F. L. *Elementary Quantum Chemistry*; McGraw-Hill: New York, 1968.

(2) Huber K. P.; Hezberg G. *Molecular Spectra and Molecular Structure. IV. Constant of Diatomic Molecules*; Von Nostrand Reinhold: New York, 1979.

(3) Kolos, W.; Roothan, C. C. *Rev. Mod. Phys.* **1960**, *32*, 327.

(4) Kutzelnigg, W.; Staemler, V.; Gélus, M. *Chem. Phys. Lett.* **1972**, *13*, 496.

(5) (a) Olson, M. L.; Konowalow, D. D. *Chem. Phys.* **1977**, *21*, 393. (b) Konowalow, D. D.; Olson, M. L. *Chem. Phys.* **1984**, *84*, 462.

(6) (a) Fernandez-Serra, P.; Bottela, V.; Smeyers, Y. G.; Galano, A.; Delgado-Barrio, G. *Int. J. Quantum Chem.* **1995**, *54*, 305. (b) Schmidt-Mink, I.; Muller, W.; Meyer, W. *Chem. Phys.* **1985**, *92*, 263. (c) Gardet, G.; Rogemond, F.; Chermette, H. *J. Chem. Phys.* **1996**, *105*, 9933. (d) Blaise, P.; Spiegelmann, F.; Maynau, D.; Malrieu, J. P. *Phys. Rev. B* **1990**, *41*, 5566.

(7) (a) Hessel, M. M.; Vidal, C. R. *J. Chem. Phys.* **1979**, *70*, 4439. (b) Verges, J.; Basic, R.; Barakat, B.; Carrot, P.; Churassy, S.; Crozet, P. *Chem. Phys. Lett.* **1983**, *98*, 203. (c) For photoassociation spectroscopy of the $^3\Sigma_u^+$ state of Cs_2, see: Fiortti, A.; Comparati, D.; Crubellier, A.; Dulieu, O.; Mansou-Seeuws, F.; Pillet, P. *Phys. Rev. Lett.* **1998**, *80*, 4402.

(8) Kaldor, U. *Chem. Phys.* **1990**, *140*, 1.

(9) Glokhovtsev, M. N.; Schleyer, P. v. R. *Isr. J. Chem.* **1993**, *33*, 455.

10.1021/ja982913n CCC: $18.00
Published on Web 03/19/1999

association spectroscopy[7c] show that no-pair bonding is a real physical situation with both fundamental and practical implications and, hence, in need of comprehension. What are the origins of no-pair bonding?

VB theory provides bonding descriptions in terms of compact wave functions involving a small number of VB structures. Since understanding the origins of no-pair bonding is a fundamental problem, we decided to undertake its VB study using the Li_2 dimer, with an aim to formulate a VB-based[6d] bonding mechanism for the no-pair situation. This paper describes the VB calculations, compares them to high-level MO-based calculations, and derives bonding mechanisms for the no-pair triplet state *vis a vis* the singlet ground state. Some insight is derived for the increase of no-pair bonding energy with cluster size and for the choice of highly symmetric geometries in these high-spin clusters (Table 1).

2. Computational Details

Since the general reader may not be familiar with notations and abbreviations used in theoretical practices, we follow with a brief explanation of the notation system, while abbreviations will be unfolded as we go along. It is common to specify a computational procedure by four principal designators, for example, QCISD(T)/6-31G*//MP2/6-31G*: The first couple of designators, separated by a slash, specify how the energy of the species is calculated, followed by a double slash and another couple of designators which specify the procedure by which the geometry of the species is calculated. Thus, the specific example means that the energy is calculated using quadratic configuration interaction calculation that includes single and double excitations with perturbative treatment of triplet excitations, QCISD(T), using the Pople basis set, 6-31G*, while the geometry is optimized with second-order Møller−Plessett (MP2) perturbation correction using the 6-31G* basis set. Additional parenthetical designators will appear to specify for example the number of electrons that are being correlated, such as in CCSD(T, full) which means that the CCSD(T) procedure involves all the electrons. Without the specification "full" the procedure excludes core electrons. In cases where only two designators appear, e.g., QCISD-(T)/6-31G*, this would mean that energy and geometry were calculated at the same level specified by the two designators. The various VB levels (see later) of computations are specified in the same manner.

Strategy. The ground and low excited states of Li_2 have been the subject of many calculations,[4−6] and several states have also been characterized experimentally.[7] Extensive ab initio computations of Li dimer were done by Kutzelnigg et al.[4] and Olson and Konowalow[5] using multiconfigurational approaches, by Meyer et al. using valence only CI with an effective core polarized potential,[6b] by Gardet et al.[6c] using density functional theory, and by Blaise et al.[6d] using an effective Hamiltonian VB technique. The lowest triplet $^3\Sigma_u^+$ state which dissociates into the ground ^{2}S terms of the Li atoms has been shown by Olson and Konowalow[5] to possess a small binding energy. Glukhovtsev and Schleyer[9] have used a QCISD(T)/6-31G*//UMP2/6-31G* level to compute states for a variety of Li_n clusters. Kaldor[8] has applied the open-shell coupled cluster method, including singles and doubles (CCSD) to calculate the potential functions of the nine lowest states of Li_2. On this background of extensive computational research, we sought for a method which can provide an accurate assessment of bond energies and serve thereby as a benchmark for the VB calculations which will eventually form a basis for an equal footing derivation of bonding mechanisms for singlet-pair and no-pair bonding.

Since the Li_2 dimer is small enough, the singlet-pair and no-pair bonding energies can be evaluated at a good degree of precision by screening a variety of sophisticated MO-based methods. Two main candidate methods are the coupled cluster level, which includes singles, doubles, and perturbational triples, CCSD(T)),[10,11] and the complete active space SCF (CASSCF) followed by second-order perturbation treatment, CASPT2.[12] The CASPT2 method is an established approach for retrieving a substantial portion of the dynamic correlation and is essential for cases with a multireference character. The CCSD(T) method has proven to be an excellent approximation to the full CI correlation energy unless the wave function exhibits distinct multireference character.[11] These methods will be employed with various basis sets, until convergence is obtained and a choice of the benchmark level can be made. Subsequently, the VB calculations will be carried out at different levels until convergence to the corresponding benchmark method can be achieved and provide thereby a reliable VB level to infer bonding mechanisms.

Basis Sets and Software for MO-Based Calculations. Correlation consistent basis sets have been specifically designed to account for as much electron correlation as possible for a given problem. As such, we used different correlation consistent basis sets ranging from cc-pVDZ to cc-pCVTZ quality; the former is a polarized double-ζ (DZ) basis set, while the latter is polarized triple-ζ (TZ) and includes the flexibility of core-valence (CV) polarization effects.[13,14] Following the literature procedure,[13] the s,p exponents of the correlation consistent basis sets were optimized in atomic Hartree−Fock (HF) calculations of the ground state. The exponents of the polarization functions were optimized at the level of configuration interaction including singles and doubles (CISD). A few Pople basis sets (6-31G, 6-31G(3d,f), 6-311G*) were also applied to the MO and VB calculations but proven less appropriate for the problem in comparison with the correlation consistent basis sets.

The Gaussian 94 suit of programs[15] was used for HF, Møller−Plessett MPn (n = 2, 4), and CCSD(T)[10] calculations. MOLCAS 2[16] was used for CASSCF[17] and CASPT2,[12] while the Utrecht package TURTLE[18] was applied for the VB calculations. TURTLE is a general nonorthogonal CI program that performs simultaneously linear variation and orbital optimization on a given set of VB configurations. The orbital optimization is based on the super-CI technique[19] related to the generalized Brillouin theorem.[20]

VB Methods. The VB wave function is represented as a linear combination of the chemical structures, Ψ_{str}, as in eq 1, where the c_{str}'s

$$\Psi_{VB} = \sum_{str} c_{str}\Psi_{str} \qquad (1)$$

are the coefficients of the VB structures. The full VB wave function is obtained by simultaneously optimizing both the coefficients of the determinants as well as all their orbitals for self-consistency. There exist two different levels to carry out this double optimization.

At the VBSCF level[18] all the orbitals are kept localized on their respective fragments and are optimized as a common orbital set for all the VB structures. The VBSCF orbitals respond therefore to a mean

(10) Raghavachari, K.; Trucks, G. W.; Pople, J. A.; Head-Gordon, M. *Chem. Phys. Lett.* **1989**, *157*, 479.

(11) Scuseria, G. E.; Lee, T. J. *J. Chem. Phys.* **1990**, *93*, 5851.

(12) (a) Andersson, K.; Malmquist, P. A.; Roos, B. O.; Sadlej, A. J.; Wolinski, K. *J. Chem. Phys.* **1990**, *94*, 5483. (b) Andersson, K.; Malmquist, P. A.; Roos, B. O. *J. Chem. Phys.* **1992**, *96*, 1218.

(13) (a) Dunning, T. H. *J. Chem. Phys.* **1989**, *90*, 1007. (b) Woon, D. E.; Dunning, T. H. *J. Chem. Phys.* **1993**, *98*, 1358.

(14) Woon, D. E. Private communication.

(15) Frisch, M. J.; Trucks, G. W.; Schlegel, H. B.; Gill, P. M. W.; Johnson, B. G.; Robb, M. A.; Cheeseman, J. R.; Keith, T. A.; Peterson, G. A.; Montgomery, J. A.; Raghavachari, K.; Al-Laham, M. A.; Zakrzewski, V. G.; Ortiz, J. V.; Foresman, J. B.; Cioslowski, J.; Stefanov, B. B.; Nanayakkara, A.; Challacombe, M.; Peng, C. Y.; Ayala, P. Y.; Chem, W.; Wong, M. W.; Andres, J. L.; Replogle, E. S.; Gomperts, R.; Martin, R. L.; Fox, D. J.; Binkley, J. S.; Defrees, D. J.; Baker, J.; Stewart, J. J. P.; Head-Gordon, M.; Gonzales, C.; Pople, J. A. *GAUSSIAN 94*, revision D.4; Gaussian Inc.: Pittsburgh, PA, 1995.

(16) Andersson, K.; Fulscher, R.; Lindh, R.; Malmqvist, P.-Å.; Olsen, J.; Roos, B. O.; Sadlej, A. J.; Widmark, P.-O. *MOLCAS*, version 2; University of Lund; Sweden, and IBM Sweden, 1991.

(17) (a) Roos, B. O.; Taylor, P. R.; Siegbahn, P. E. M. *Chem. Phys*. **1980**, *48*, 157. (b) Siegbahn, P. E. M.; Almlof, J.; Heiberg, A.; Roos, B. O. *J. Chem. Phys*. **1981**, *74*, 2384.

(18) Verbek, J.; Langenberg, J. H.; Byrman, C. P.; Dijkstra, F.; van Lenthe, J. H. *TURTLE-An ab initio VB/VBSCF program*; University of Utrecht: Utrecht, the Netherlands, 1997.

(19) (a) Grein, F.; Chang, T. C. *Chem. Phys. Lett.* **1971**, *12*, 44. (b) Banerjee, A.; Grein, F. *Int. J. Quantum Chem.* **1976**, *10*, 123.

(20) Levy, B.; Berthier, G. *Int. J. Quantum Chem.* **1968**, *2*, 307.

field of the set of VB structures, i.e., to an averaged atomic situation over the atomic states used in the VB structure set.

At the BOVB level[21a,b,c] this mean-field constraint is removed and each VB structure is allowed to have its own specific orbitals. As a result, the optimized orbitals are different from one structure to the other due to instantaneous response of the electrons to the local fields of the individual structures. The orbitals can be viewed as following the electronic fluctuation by rearranging in size and shape, hence the name "breathing-orbital valence bond" (BOVB). Thus, the BOVB wave function accounts for some dynamic correlation during the bonding in response to the charge fluctuation specified by the chemical nature of VB structures. There are levels of BOVB which differ in sophistication.[22] With a single exception, specified later, the present paper uses the simplest form which employs orbitals (atomic or hybrids) which are localized on given atomic centers. The orbitals which are allowed to breath during the optimization procedure are the valence 2s and 2p orbitals, whereas the 1s core orbitals are kept at their VBSCF optimized situations. The BOVB and VBSCF geometry optimization was carried out with 0.1 Å steps because TURTLE lacks the facility of an automated geometry optimization.

When a single VB structure is allowed to optimize by itself, we obtain the variational energy of that structure. Having variational energies of individual structures enables one to define variational values for conceptually important quantities such as covalent bond energy and VB mixing energy.

An alternative modern VB approach is provided by the general valence bond (GVB)[21d] or spin-coupled VB (SCVB)[21e] theories, in which an electron pair is described by a single VB structure, formally covalent but with orbitals that are allowed to delocalize freely and that might be considered as distorted atomic orbitals. With minimal basis sets, the GVB/SCVB wave functions of a singlet electron-pair bond implicitly contain localized covalent and ionic structures which are explicitly used in the traditional VBSCF wave function, and therefore, all the wave functions (VBSCF and GVB/SCVB) are nearly equivalent. Both VBSCF and GVB/SCVB theories are however less accurate[21a−c] than BOVB for singlet electron-pair bonds. For the problem of no-pair bonding, the GVB method did not reveal a minimum, while VBSCF gave a minimum close enough to the benchmark method, CCSD(T).

3. Results

3.1. MO-Based Calculations. An initial test showed that the $^2S \rightarrow {}^2P$ excitation energy of the Li atom can be reproduced[23] very well at the CCSD(T,full) level with all correlation consistent basis sets.[24]

For the excited states of Li_2 we tested all computational levels starting with Hartree−Fock self-consistent field (HF−SCF) theory. No minimum was found for the $^3\Sigma_u^+$ state of Li_2 at the HF−SCF level of theory with any of the basis sets used in this study. This means that no-pair bonding is not a simple outcome of s−p orbital hybridization which is optimal at the SCF orbital level but rather a result of some correlation effect which is necessary to describe correctly the no-pair state. Some tests with MPn (n = 2, 4)[15] were carried out and showed that these methods were still inappropriate to describe no-pair bonding.[24]

Table 2. Equilibrium Distances R_e (Å) and Bond Energies D_e (eV) Calculated at the CASSCF[a] and CASPT2 Levels of Theory for Different States of Li_2

			CASSCF		CASPT2	
entry	state	basis	D_e	R_e	D_e	R_e
1a	$^1\Sigma_g^+$	cc-pVDZ	0.975	2.7	0.982	2.7
1b		cc-pVTZ	0.983	2.7	1.009	2.7
1c		exp[b]	1.056	2.673		
2a	$^3\Pi_u$	cc-pVDZ	1.373	2.6	1.428	2.6
2b		cc-pVTZ	1.410	2.6	1.493	2.6
2c		exp[b]	1.510	2.591		
3	$^3\Sigma_g^+$	cc-pVDZ	0.768	3.2	0.798	3.2
4	$^3\Sigma_u^+$	cc-pVDZ	0.0246	4.2	0.0316	4.2

[a] The orbitals $1\sigma_g 1\sigma_u 2\sigma_g 2\sigma_u\ 1\pi_u\ 2\pi_u 3\sigma_g 3\sigma_u 1\pi_g\ 2\pi_g$ were included in the active space for CASSCF. [b] From ref 8.

Thus, the correlation effects were examined by employing the CASSCF,[17] CASPT2,[12] and CCSD(T)[10] methods.

CASSCF and CASPT2 results for four Li_2 states are collected in Table 2. Static electron correlation (in CASSCF) is required to establish a minimum for the no-pair bond.

Dynamic correlation effects (in CASPT2) have no influence on the equilibrium distance (R_e) for all states. In contrast, dynamic correlation increases the bond energies (D_e) for all the states and by ca. 30% for the $^3\Sigma_u^+$ state.

The results of the CCSD(T,full) calculations for different states of the Li_2 dimer are summarized in Table 3 along with previous results. It is seen that using a triple-ζ (TZ) basis sets, and especially with core-valence polarization, cc-pCVTZ, leads to results which are virtually identical (within 1%) to the experimental data for D_e, R_e, and the harmonic frequencies (ω). The CCSD(T,full)/cc-pCVTZ results agree with experiment even better than the corresponding CASPT2 results shown in Table 2 and many others which have been tried (using the ANO-s basis set)[24] and are not shown here. Additional tests showed that the correlation consistent basis sets are probably more suitable for the no-pair state than Pople's 6-311G* basis set.[24] Boys−Bernardi[25] counterpoise correction calculation showed that basis set superposition error (BSSE) for CCSD(T,full) calculations of the $^3\Sigma_u^+$ state of Li_2 is in the range of 0.000 57−0.000 67 eV for all correlation consistent basis sets.[24] Furthermore BSSE was found to be negligible (0.000 09−0.000 67 eV) at all levels ranging from HF onward to CCSD(T), and while there is no good way to estimate BSSE at our VB levels, it is reasonable to expect that they would also show negligible BSSE.

The foregoing discussion reveals that the CCSD(T) method in combination with correlation consistent basis sets is most reliable for the Li_2 dimer problem and can serve as a reference benchmark for the VB calculations of the $^3\Sigma_u^+$ state where no experimental data are yet available.

3.2. Results of VB Calculations. VBSCF Results for the $^3\Sigma_u^+$ No-Pair Bond State. Figure 1 depicts the VB structures which are nascent from the fundamental triplet covalent configuration, $^3\Phi_{ss}$ (a in Figure 1), by distributing the triplet electron pair among the valence orbitals in manners which correspond to the requisite $^3\Sigma_u^+$ state symmetry. As can be seen, the VB structure-set involves four covalent configurations (a and c−e in Figure 1) and two ionic ones (b in Figure 1), much like the VB structures that would describe an electron-pair bond,[26] except that the electrons maintain a triplet relation-

(21) (a) Hiberty, P. C.; Flament, J. P.; Noizet, E. *Chem Phys. Lett*. **1992**, *189*, 259. (b) Hiberty, P. C.; Humbel, S.; Byrman, C. P.; van Lenthe, J. H. *J. Chem. Phys.* **1994**, *101*, 5969. (c) Hiberty, P. C.; Humbel, S.; Archirel, P. *J. Phys. Chem.* **1994**, *98*, 11697. (d) Bobrowicz, F. W.; Goddard, W. A., III. In *Modern Theoretical Chemistry: Methods of Electronic Structure Theory*; Schaefer, H. F., III, Ed.; Plenum: New York, 1997; Vol. 3, p 79. (e) Cooper, D. L.; Gerratt, J.; Raimondi, M. In *Valence Bond Theory and Chemical Structure*; Klein, D. J., Trinajstic, N., Eds.; Elsevier: Amsterdam, 1990; p 287.

(22) For a recent review of the method, see: Hiberty, P. C. In *Modern Electronic Structure Theory and Applications in Organic Chemistry*; Davidson, E. R., Ed.; World Scientific: River Edge, NJ, 1997; pp 289−367.

(23) Moore, C. E. *Atomic Energy levels*; NSRDS−NBS: U.S. GPO 35, Washington, DC, 1971.

(24) Unpublished data: available from authors upon request.

(25) Boys, S. F.; Bernardi, F. *Mol. Phys*. **1970**, *19*, 553.

(26) (a) Shaik S. In *New Concepts for Understanding Organic Reactions*; Bertran, J., Csizmadia, I. G., Eds.; NATO ASI Series; Kluwer: Dordrecht, The Netherlands, 1989; Vol. C267. (b) Shaik, S.; Hiberty, P. C. *Adv. Quantum Chem.* **1995**, *26*, 99.

Table 3. Equilibrium Distances R_e (Å), Harmonic Frequencies ω (cm^{-1}), and Bond Energies D_e (eV) Calculated at the CCSD(T,full) Level of Theory for Different States of Li_2

entry		cc-pVDZ	cc-pCVDZ	cc-pVTZ	cc-pCVTZ	CCSD[a]	ECPP−CI[b]	exp[a]
1	$^1\Sigma_g^+$							
a	R_e	2.712	2.697	2.667	2.680	2.67	2.675	2.673
b	ω	335.25	246.61	344.20	348.77	351.0	351.0	351.40
c	D_e	0.983	1.011	1.058	1.039	1.061	1.050	1.056
2	$^3\Pi_u$							
a	R_e	2.612	2.610	2.574	2.594	2.58	2.595	2.591
b	ω	329.84	345.22	341.98	346.03	349.0	345.6	345.7
c	D_e	1.450	1.462	1.520	1.496	1.510	1.506	1.510
3	$^3\Sigma_u^+$							
a	R_e	4.188	4.152	4.103	4.193	4.06	4.182	
b	ω	64.92	66.84	69.92	65.24	75.0	63.7	
c	D_e	0.0324	0.0339	0.0456	0.0391	0.038	0.0399	
4	$^3\Sigma_g^+$							
a	R_e	3.152	3.133	3.083	3.089	3.06	3.067	
b	ω	244.0	247.56	243.49	246.24	252.0	252.2	
c	D_e	0.817	0.833	0.859	0.847	0.876	0.877	

[a] From ref 8. [b] ECPP stands for effective core polarization potential. The CI includes valence-only CI. From ref 6b.

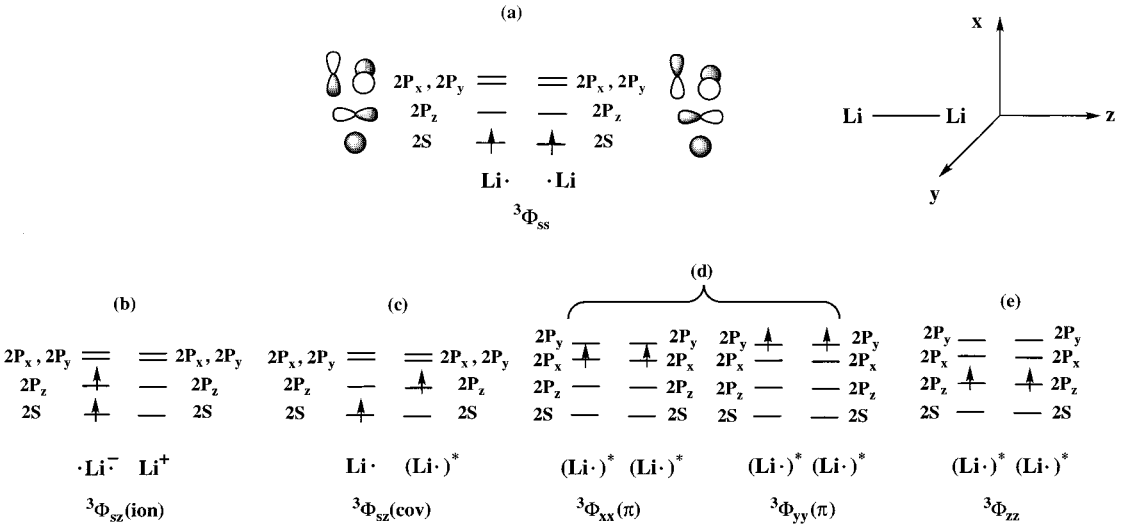

Figure 1. VB structure-set for the $^3\Sigma_u^+$ state of Li_2. $^3\Phi_{sz}$(cov) and $^3\Phi_{sz}$(ion) each have an additional symmetry-related structure which is not shown.

Table 4. VBSCF/cc-pVDZ Calculated Properties of the No-Pair $^3\Sigma_u^+$ State of Li_2[a]

entry	configurations	R_e (Å)	D_e (eV)
1	$^3\Phi_{ss}$	repulsive	repulsive
2	$^3\Phi_{ss} + {}^3\Phi_{sz}$(ion)	repulsive	repulsive
3	$^3\Phi_{ss} + {}^3\Phi_{sz}$(ion) + $^3\Phi_{zz}$	5.4	0.0070[b]
4	$^3\Phi_{ss} + {}^3\Phi_{sz}$(ion) + $^3\Phi_{zz} + {}^3\Phi_{xx}(\pi) + {}^3\Phi_{yy}(\pi)$	4.5	0.0220[b]
5	$^3\Phi_{ss} + {}^3\Phi_{sz}$(ion) + $^3\Phi_{zz} + {}^3\Phi_{xx}(\pi) + {}^3\Phi_{yy}(\pi)$	4.4	0.0294[c]

[a] The configurations refer to Figure 1. [b] The same value is obtained if $^3\Phi_{sz}$(cov) replaces $^3\Phi_{zz}$ or if both are simultaneously included. With $^3\Phi_{zz}$ energy convergence is faster. [c] This is a VBSCF/cc-pCVTZ datum.

Table 5. BOVB/cc-pVDZ Calculated Properties of the No-Pair $^3\Sigma_u^+$ State of Li_2[a]

entry	configurations	R_e (Å)	D_e (eV)
1	$^3\Phi_{ss}$	repulsive	repulsive
2	$^3\Phi_{ss} + {}^3\Phi_{sz}$(ion)	6.7	0.0006
3	$^3\Phi_{ss} + {}^3\Phi_{sz}$(ion) + $3\Phi_{xx}(\pi) + {}^3\Phi_{yy}(\pi)$	5.8	0.0030
4	$^3\Phi_{ss} + {}^3\Phi_{sz}$(ion) + $^3\Phi_{zz}$	4.9	0.0096[b]
5	$^3\Phi_{ss} + {}^3\Phi_{sz}$(ion) + $^3\Phi_{zz} + {}^3\Phi_{xx}(\pi) + {}^3\Phi_{yy}(\pi)$	4.3	0.0277 (0.0324)[b,c]

[a] The configurations refer to Figure 1. [b] The same value is obtained if $^3\Phi_{sz}$(cov) replaces $^3\Phi_{zz}$ or if both are simultaneously included. With $^3\Phi_{zz}$ energy convergence is faster. [c] In parentheses is the CCSD(T,full)/cc-pVDZ datum.

ship. Ionic π-structures are not depicted since a test (Table 6, entry 6) shows their dismal effect on bonding. In either the VBSCF or BOVB procedures the 2s and $2p_z$ orbitals are allowed to hybridize freely, and at the end of the procedure $^3\Phi_{ss}$ has 2s hybrids which involve a small $2p_z$ character, while $^3\Phi_{zz}$ or $^3\Phi_{sz}$(cov) possess $2p_z$ hybrids which contain some 2s character. The degree of hybridization is not identical nor does it correspond to any simple hybridization model (in accord with Blaise et

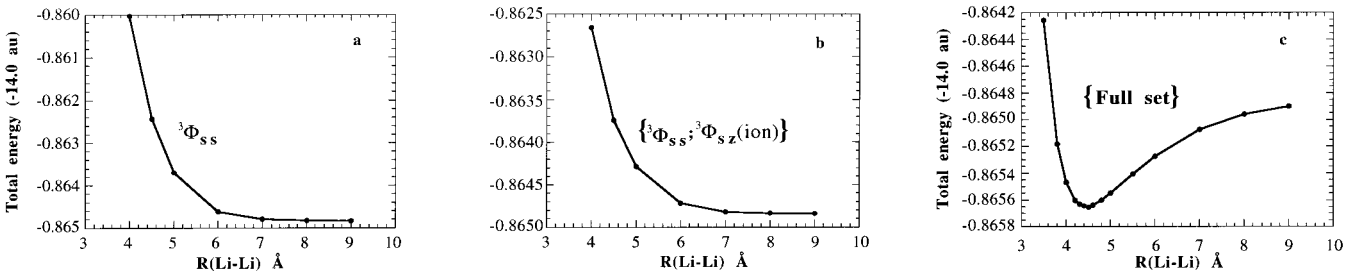

Figure 2. VBSCF/cc-pVDZ energy curves for the $^3\Sigma_u^+$ state of Li_2: (a) repulsive $^3\Phi_{ss}$ curve; (b) repulsive $\{^3\Phi_{ss}, ^3\Phi_{sz}(ion)\}$ curve; (c) curve for the full VB structure-set excluding the redundant structure.

Table 6. Comparison of BOVB/Basis-Set Results for the $^3\Sigma_u^+$ State of Li_2[a]

entry	basis set	R_e (Å)	D_e (eV)
1	BOVB/6-31G*	4.5	0.0251
2	BOVB/cc-pVDZ	4.3	0.0277
3	BOVB/cc-pCVDZ	4.3	0.0286
4	BOVB/cc-pVTZ	4.3	0.0349
5	BOVB/cc-pCVTZ	4.3	0.0350
6	BOVB(full)/cc-pCVTZ[b]	4.25	0.0385
7	CCSD(T,full)/cc-pCVTZ[c]	4.19	0.0391

[a] The VB structure-set involves $^3\Phi_{ss}$, $^3\Phi_{sz}$(ion), $^3\Phi_{zz}$, $^3\Phi_{xx}$, and $^3\Phi_{yy}$. [b] BOVB(full) corresponds to a calculation where the π-charge transfer configurations are implicitly included in the configuration set. This was achieved by allowing the p_π AO's of the covalent π-configurations to delocalize freely as in GVB.[21d] [c] Core electrons were included in the CCSD(T) calculations.

al.[6d]), and since the hybrid orbitals of the VB structures still resemble their AO parents, we prefer to retain the original labels of Figure 1 and refer to the orbitals as 2s and $2p_z$.

A full VBSCF treatment of the complete set of VB structures showed that the set is saturated and the total energy does not change if either $^3\Phi_{sz}$(cov) or $^3\Phi_{zz}$ are removed from the calculation. This saturation is associated with the hybridization which renders the $^3\Phi_{sz}$(cov) and $^3\Phi_{zz}$ configurations redundant. Thus, the VBSCF calculations exhibit *a convergence behavior* with respect to the set of configurations nascent from the valence orbitals.

The individual roles of the configurations are summarized in Figure 2 and Table 4. The fundamental triplet covalent structure $^3\Phi_{ss}$ (a in Figure 1) was chosen as a reference configuration. To this structure we added successively the other VB structures, in a manner which allows one to specify the individual effects and combinations thereof. These partial VBSCF calculations used the cc-pVDZ basis set.

The $^3\Phi_{ss}$ potential energy curve is presented in the Figure 2a and is seen to be repulsive with no minimum, much like in the $^3\Sigma_u^+$ state for H_2. Figure 2b shows that the VBSCF energy curve for a wave function which involves $^3\Phi_{ss}$ and the two ionic configurations $^3\Phi_{sz}$(ion) is still repulsive. Adding the π-type structures $^3\Phi_{xx(yy)}$ makes little difference. The essential VB combination with an incipient no-pair bonding involves $^3\Phi_{ss}$ and $^3\Phi_{sz}$(ion) with either $^3\Phi_{sz}$(cov) or $^3\Phi_{zz}$. Each one of these combinations leads to a minimum and a finite bond energy, albeit still off relative to the benchmark calculation. Thus, Figure 2c shows the energy curve for the full VBSCF wave function which is spanned by the nonredundant VB structures. This energy curve exhibits a minimum at 4.5 Å and a no-pair bonding of 0.0220 eV (entry 4, Table 4), which is very similar to the CASSCF D_e value in Table 2. VBSCF/cc-pCVTZ calculation further improves the result to 0.0294 eV (entry 5, Table 4) and shifts the equilibrium distance to 4.4 Å. Thus, valence orbital correlation is necessary to account for no-pair bonding, and the configurations which are essential to produce a minimum are the ionic $^3\Phi_{sz}$(ion) and covalent $^3\Phi_{sz}$(cov)/$^3\Phi_{zz}$ structures. Interestingly, the GVB method, which should have implicitly contained the essential configurations, through the orbital delocalization tails, shows no minima. Apparently, the flexibility of the VBSCF procedure that enables each configuration to possess its own variational coefficient is essential to describe the no-pair bond.

BOVB Results for the $^3\Sigma_u^+$ No-Pair Bond State. Examination of the VB structures in Figure 1 shows that the occupied orbitals feel different fields which are characteristics of the respective VB structure. For example, the 2s orbital in the ionic structure (b in Figure 1) feels the field of the $2p_z$ electron, which is different than the field felt by the 2s orbital of the covalent structure (a in Figure 1). This would cause a dynamic change in the shape of the 2s hybrid orbital of the ionic configurations that should adopt its size and hybridization to the local field of the Li species in the respective configuration. This dynamic effect can be accounted for by use of the BOVB approach,[21a−c] which retains the compactness of the VBSCF wave function, but can improve the energetics by dressing the VB structures with dynamic correlation. Inspection of the orbitals obtained by VBSCF and BOVB demonstrates that the two procedures yield orbitals which are nearly identical in terms of shape and hybridization for the covalent structure, whereas orbitals which correspond to the ionic structures have a greater degree of sp_z-hybridization in the BOVB procedure in line with findings by Blaise et al.[6d]

Figure 3a−d shows the potential energy curves for the various BOVB wave functions while Table 5 collects the corresponding D_e and R_e values. As in VBSCF, the BOVB calculation with the full VB structure-set shows that the $^3\Phi_{zz}$ and $^3\Phi_{sz}$(cov) structures are redundant and the energy exhibits convergence with respect to the structure-set generated from the valence orbitals. It is important to note that, as long as the calculations involve no redundant configurations, the BOVB wave function exhibits a remarkably stable behavior with respect to the coefficients, overlaps, and reduced matrix elements of its constituent structures.

Much like the VBSCF behavior here too, the fundamental structure $^3\Phi_{ss}$ is repulsive (see Figure 2a). However, unlike the VBSCF, here with BOVB the mixing of covalent and ionic VB structures already leads to emergence of no-pair bonding, seen in Figure 3a and entry 2 in Table 5. Repeating the BOVB procedure, while adding the π-type $^3\Phi_{xx(yy)}$ structures, shifts the minimum to a shorter distance (5.8 Å) and increases bonding energy to 0.003 eV (Figure 3b and entry 3 in Table 5). Figure 3c shows the energy curve which results by adding to the fundamental covalent and ionic structures also the $^3\Phi_{zz}$ configuration. It is apparent that, in comparison with the previous step, the equilibrium distance undergoes considerable shortening to 4.9 Å, and the no-pair bonding energy increases more than

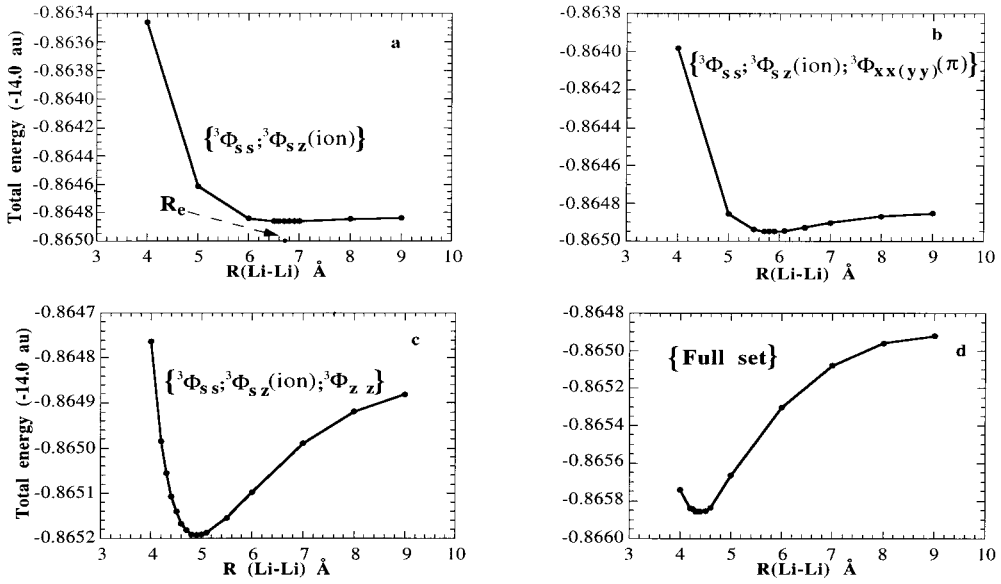

Figure 3. BOVB/cc-pVDZ energy curves for the $^3\Sigma_u^+$ state of Li_2. The repulsive $^3\Phi_{ss}$ curve is the same as in Figure 2a: (a) {$^3\Phi_{ss}$, $^3\Phi_{sz}$(ion)} curve with the incipient energy minimum at 6.7 Å; (b) {$^3\Phi_{ss}$, $^3\Phi_{sz}$(ion), $^3\Phi_{xx(yy)}(\pi)$} curve; (c) {$^3\Phi_{ss}$, $^3\Phi_{sz}$(ion), $^3\Phi_{zz}$} curve; (d) curve for the full VB structure-set excluding the redundant structure.

three times, to 0.0096 eV (entry 4, Table 5). We note that inclusion of the $^3\Phi_{zz}$ covalent configuration here is equivalent to the introduction of contributions due to double excitations [($s_a \rightarrow p_{z_a}$)($s_b \rightarrow p_{z_b}$)] in a correlated MO treatment.[4,5,6b,8] The final step presented in Figure 3d shows the energy curve for the BOVB wave function that includes all the structure-set with exclusion of redundancy. The resulting minimum for the no-pair bond is located now at 4.3 Å while the bond energy becomes 0.0277 eV (entry 5, Table 5), in good agreement with the corresponding CCSD(T) result in the same basis set.

The basis set effect on the BOVB no-pair bonding energy is presented in the Table 6. First, it appears that correlation consistent basis sets are more suitable for BOVB calculations than Pople's type basis sets (entry 1). Second, for all the basis sets with the correlation consistent quality (entries 2−6), the equilibrium distance is not sensitive to the basis set within the 0.1 Å range of accuracy of the geometry optimization procedure. Third, core-valence polarization effect has little effect on the bond energy using the correlation consistent basis set (entries 2 vs 3 and 4 vs 5). The TZ basis set with the core-valence polarization feature (entries 5 vs 7) leads to a result which is very close to the CCSD(T,full)/cc-pCVTZ one. Further inclusion of the missing π-type charge-transfer structures in entry 6 of Table 6 brings the BOVB and CCSD(T,full)/cc-pCVTZ results to virtual identity.

In summary, the VBSCF wave function is qualitatively correct, much like the CASSCF wave function, both reflecting the importance of nondynamic correlation to the establishment of no-pair boding. The BOVB wave function of the no-pair bond is both qualitatively correct and quantitatively accurate and reflects the importance of dynamic correlation to the energetics and equilibrium distance of the no-pair bond. Both the BOVB and the VBSCF results project that, among the secondary structures, the key ones are $^3\Phi_{sz}$(ion) and $^3\Phi_{zz}/^3\Phi_{sz}$(cov) which by mixing into the fundamental covalent structure $^3\Phi_{ss}$ generate an incipient no-pair bond.

BOVB Results for the $^1\Sigma_g^+$ Ground State: To compare the no-pair bonding mechanism to the corresponding singlet-pair bonding, we carried out BOVB calculations of the $^1\Sigma_g^+$ ground singlet state of Li_2. The VB structure-set is shown in Figure 4, which depicts in a the fundamental structure $^1\Phi_{ss}$, and the nascent configurations which distribute the singlet-pair in the valence orbitals. In e we grouped all the structures which are redundant with $^1\Phi_{zz}$(cov). Thus here, too, due to the 2s−2p_z hybridization, the VB structure-set is saturated with respect to the valence orbitals, and the contribution of all the redundant set is no more than 0.7% of the total bond energy.

The results for the various BOVB wave functions are collected in the Table 7. Entry 1 shows the optimum values for a BOVB wave function which includes only the $^1\Phi_{ss}$ covalent structure, known also by the name the Heitler−London configuration.[26] The covalent structure gives us about half of the experimental bond energy value and an R_e value slightly longer than experiment (entry 10, Table 7). Clearly, unlike the triplet state calculations, in the ground state the singlet-pairing of $^1\Phi_{ss}$ is significantly bonded, as expected for a singlet-pair.[26] Inclusion of the lowest ionic configurations $^1\Phi_{ss}$(ion) (Table 7, entry 2) improves the results by ca. 25%. Very little further improvement is conferred by adding the $^1\Phi_{zz}$(cov) structure (entry 3, Table 7). Thus, in all, the singlet-pairing along with the associated ionic fluctuations contributes ca. 64% of the bond energy.

The contribution of π-bonding is apparent from entry 4 in Table 7 which shows a substantial improvement of the bonding energy upon addition of the $^1\Phi_{xx}(\pi)$ and $^1\Phi_{yy}(\pi)$ structures. In fact, π-bonded structures are more important than the ionic structures, which is not the case for a bond like H−H or C−H, etc. Removal of the ionic configurations, while retaining all the covalent configurations, yields about 98% of the total bonding energy obtained with the full VB structure-set. The agreement with experiment improves on utilization of the cc-pCVTZ basis set, resulting in a bond energy value (entry 7, Table 7) within 7% compared with experimental and the CCSD(T,full) values. As in the case of the $^3\Sigma_u^+$ state of Li_2, here too inclusion of π-type charge-transfer configurations brings the agreement between BOVB and CCSD(T,full) to within 4% (entry 8).

4. Discussion

Application of VB theory reveals some similarities along with key differences in the features of the singlet-pair and no-pair bonds of Li_2. The similarity is apparent from the common

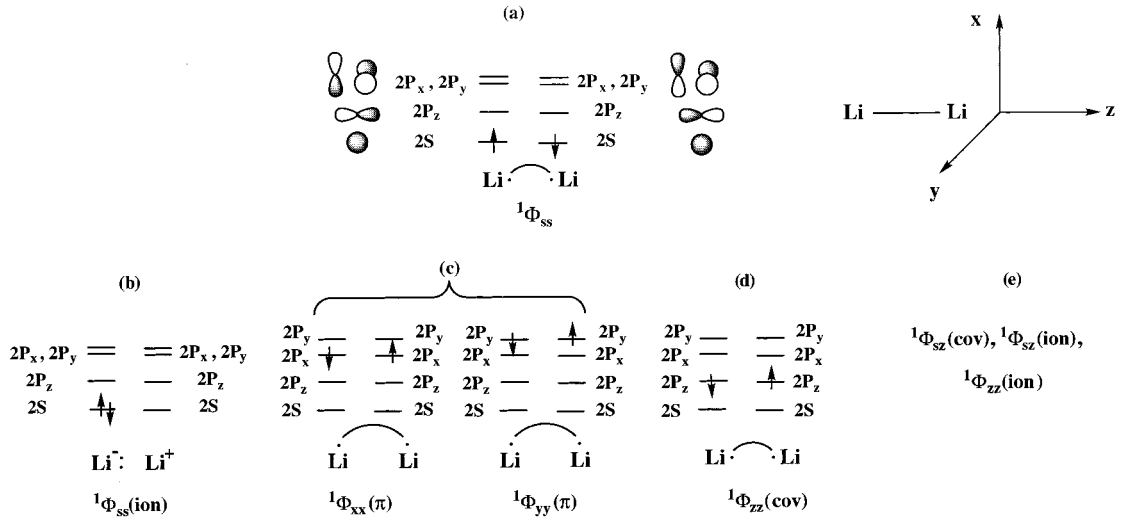

Figure 4. VB structure-set for the $^1\Sigma_g^+$ ground singlet state of Li_2. Only one structure of each symmetry-related pair is depicted (e.g., $^1\Phi_{ss}$(ion)). In (e) we show the structures which are redundant with $^1\Phi_{zz}$(cov).

Table 7. BOVB/cc-pVDZ and BOVB/cc-pCVTZ Properties of the $^1\Sigma_g^+$ State of Li_2

entry	configurations[a]	R_e (Å)	D_e (eV)
1	$^1\Phi_{ss}$	2.95	0.413
2	$^1\Phi_{ss} + {}^1\Phi_{ss}$(ion)	2.9	0.566
3	$^1\Phi_{ss} + {}^1\Phi_{ss}$(ion) + Φ_{zz}(cov)	2.9	0.575
4	$^1\Phi_{ss} + {}^1\Phi_{xx}(\pi) + {}^1\Phi_{yy}(\pi)$	2.7	0.766
5	$^1\Phi_{ss} + {}^1\Phi_{xx}(\pi) + {}^1\Phi_{yy}(\pi) + \Phi_{zz}$(cov)	2.7	0.883
6	$^1\Phi_{ss} + {}^1\Phi_{ss}$(ion) + $^1\Phi_{xx}(\pi) + {}^1\Phi_{yy}(\pi) + \Phi_{zz}$(cov)	2.7	0.897[b]
7	$^1\Phi_{ss} + {}^1\Phi_{ss}$(ion) + $^1\Phi_{xx}(\pi) + {}^1\Phi_{yy}(\pi) + \Phi_{zz}$(cov)	2.7	0.978[c]
8	BOVB(full)/cc-pCVTZ	2.7	1.011[d]
9	CCSD(T,full)/cc-pCVTZ	2.68	1.039
10	exp[e]	2.673	1.056

[a] The configurations refer to Figure 4. [b] Adding all the redundant configurations changes the result by ca. 0.007 eV. [c] BOVB/cc-pCVTZ result. [d] BOVB calculation (6 configurations as in entry 7). BOVB(full) corresponds to a calculation where the π-charge-transfer configurations ($^3\Phi_{xx}(\pi$-CT) and $^3\Phi_{yy}(\pi$-CT)) are also implicitly included in the configuration set by allowing the p_π AO's in the covalent structures to delocalize freely as in GVB.[21d] [e] From ref 8.

Table 8. BOVB/cc-pVDZ Coefficients in the Wave Functions of the $^3\Sigma_u^+$ and $^1\Sigma_g^+$ States of Li_2

entry	configurn[a]	$^3\Sigma_u^+$ [b]	$^1\Sigma_g^+$ [b]
1	Φ_{ss}(cov)	0.97214	0.977168
2	Φ(ion)	0.068157 (−7.6514 [**m**])	−0.085206 (+27.80341 [**b**])
		−0.068157	−0.085206
3	Φ_{zz}(cov)	−0.110778 (+10.3719 [**m**])[c]	0.025435 (+8.430265 [**m**])[c]
4	$\Phi_{xx}(\pi)$	−0.050136 (+5.054 [**b**])	−0.169427 (+27.04675 [**b**])
5	$\Phi_{yy}(\pi)$	−0.050136	−0.169427

[a] The configurations refer to Figures 1 and 4. [b] In parentheses are reduced matrix elements (kcal/mol) of unique structures (β_i in eq 3). [**m**] and [**b**] refer to monoelectronic and bielectronic, respectively. [c] The $\langle\Phi_{ss}|\Phi_{zz}\rangle$ overlap is negatively signed.

description of the bonding in terms of mixing of a set of covalent and ionic VB structures. The differences are, however, rooted in the precise nature of the two bonding mechanisms. Before discussing the individual bonding mechanisms, it is instructive to inspect the BOVB wave function in Table 8. It is apparent that, in both states, the single dominant configuration is Φ_{ss}, while all the others have very small coefficients which indicate that, in each state, bonding arises from a perturbative VB mixing into the fundamental configuration, as depicted schematically in Figure 5a.

Following Figure 5a, the bond energy can be expressed as eq 2, where $^{1,3}E_{ss}$ is the energy of the fundamental configuration

$$D = -(^{1,3}E_{ss} - 2E_{Li}) - \Delta E_{mix} \qquad (2)$$

and $2E_{Li}$ is the corresponding energy of the separated Li atoms, while ΔE_{mix} is the VB mixing term. Figure 5b,c compares these quantities (BOVB/cc-pVDZ values) using the variationally optimized $^{1,3}E_{ss}$ energies as a reference. It is apparent that $^1\Phi_{ss}$ is significantly bonded, and the VB mixing term provides ca. 50% of the singlet-pair bond energy, while $^3\Phi_{ss}$ is repulsive and the no-pair bonding arises solely due to the VB mixing term.

To discuss the two bond types in line of eq 2, it is necessary to specify the behavior of the VB mixing term. As already stated, our analysis shows that ΔE_{mix} can be reproduced quite accurately using second-order perturbation theory, i.e.,

$$\Delta E_{mix} = \sum_i c_i\beta_i \quad \beta_i = H_{i,ss} - E_{ss}S_{i,ss} \qquad (3)$$

Here, β_i is the reduced matrix element that is the effective matrix element responsible for the VB mixing[26] and c_i is the mixing coefficient of the ith secondary VB structures.[27]

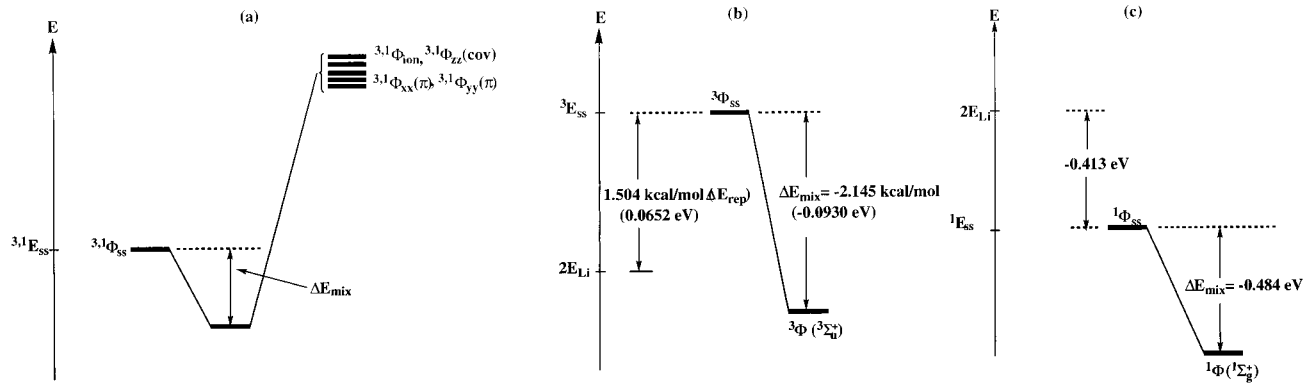

Figure 5. (a) Schematic VB mixing diagram showing the perturbative energy lowering of the fundamental structure $^{1,3}\Phi_{ss}$(cov) due to its mixing with all the nonredundant secondary structures. (b) Repulsive and mixing energies in the no-pair $^3\Sigma_u^+$ state. (c) Covalent bonding and mixing energies in the $^1\Sigma_g^+$ state. Due to the order of magnitude difference, the energies in (b) are expressed in kcal/mol while in (c) they are expressed in eV.

Table 8 indicates in parentheses the reduced matrix elements, and one can distinguish two types denoted by **[m]** and **[b]**, which stand for monoelectronic and bielectronic, respectively. As a rule, if all overlap integrals are taken as positive, then a monoelectronic β_i will be a negative quantity when the overlap is positively signed and positive when the overlap is negatively signed.[26] A bielectronic β_i is always positive when the overlap is either zero or positively signed. Inspection of Table 8 shows that the reduced matrix elements of the π-type configurations are always bielectronic since these structures have a zero overlap with the fundamental structure.[28a] Interestingly the singlet ionic structures possess a positive reduced matrix element that is formally assigned a bielectronic nature.[28b] All other structures have monoelectronic matrix elements.

The nature of the reduced matrix element carries some chemical significance. Thus, the monoelectronic matrix element is associated with electron-hops between the overlapping orbitals and as such corresponds to the classical one electronic resonance interaction between VB structures.[26] On the other hand, the bielectronic matrix element is associated with the classical improvement of Coulomb correlation of the electrons.[28b] Using this information, we turn to discuss the two bonding types of the singlet ground state and the triplet no-pair state.

Singlet-Pair Bonding in the $^1\Sigma_g^+$ State of Li_2. Inspection of Table 8 shows that the ΔE_{mix} term will be dominated by the π-bonded structures, with a smaller contribution from the ionic structures and a dismal one from the covalent $^1\Phi_{zz}$ structure which consequently can be disregarded. Thus, the ionic and π-structures mix into the fundamental structure, $^1\Phi_{ss}$, to improve the Coulomb correlation of the electron pair. If we separate the contribution of the ionic structure from that of the π-type structure, we can express the singlet bond energy as a sum of σ-pairing bond energy (eq 4a) and a Coulomb correlation term

$$D_{\sigma-\text{pairing}} = D_{\text{cov}} - \Delta E_{\text{mix}}(\text{ion})$$
$$\Delta E_{\text{mix}}(\text{ion}) = \dot{\sigma}\text{-Coulomb correlation} \quad (4a)$$

$$D = D_{\sigma-\text{pairing}} + 0.16943(K_{sx} + K_{sy})$$
$$c = -0.16943 \text{ (Table 8)} \quad (4b)$$

due to the mixing of the $\Phi(\pi)$ configurations (eq 4b). The latter is given by the product of the coefficient and the reduced matrix element which is simply a sum of bielectronic exchange integrals, K_{sx} and K_{sy}.[28a] Accordingly the bond energy becomes eq 4b. It follows, therefore, that singlet-pairing in the $^1\Sigma_g^+$ state *is primarily* σ-type covalent-pairing, augmented by Coulomb correlation through the dispersion of the electron-pair into the π-bonding orbitals.[29]

No-Pair Bonding in the $^3\Sigma_u^+$ State. As may be seen from Figure 5b, the fundamental structure, $^3\Phi_{ss}$, of the no-pair state is repulsive due to the triplet interaction of the electrons, and the no-pair bond originates in the VB mixing term. The corresponding bond energy can be rewritten as a balance between the VB mixing term and the triplet-pair repulsion, eq 5.

$$D_{\text{no-pair}} = -\Delta E_{\text{mix}} - \Delta E_{\text{rep}}(^3\Phi_{ss}) \quad (5)$$

Using the data in Table 8 shows that the two $^3\Phi_{sz}$(ion) ionics and the single $^3\Phi_{zz}$ covalent structures contribute together ca. 81% of the VB mixing term, and their contribution is due to monoelectronic resonance terms. *It follows therefore that no-pair bonding originates in the balance between the triplet repulsion of the s−s triplet pair and the resonance energy due to the mixing of the ionic and covalent* σ-type VB structures. While the resonance energy contribution due to mixing of the ionic structures can be understood in terms of the classical monoelectronic resonance interaction associated with one electron hoping, that of the $^3\Phi_{zz}$ is bit more tricky and can be understood in two complementary ways.[30a,b] Thus, using the rules of VB mixing,[26] it can be shown that $^3\Phi_{ss}$ and $^3\Phi_{zz}$ are coupled by a matrix element analogous to that which is responsible for the covalent energy of a singlet structure.[30a] In this sense, the mixing of $^3\Phi_{zz}$ adds a monoelectronic covalent

(27) From perturbation theory, the coefficient itself is given by $c_i = \beta_i/(E_{ss} - E_i)$.

(28) (a) This is a simple outcome of Slater rules for matrix elements between determinant wave functions. (b) The fundamental and the ionic structures of the ground state differ by one electron hoping between two hybrid AO's, and their matrix element is the well-known hoping integral which is negative and dominated by the monoelectronic part of the Hamiltonian. However, we recall that, in VB theory, the VB mixing is dominated by the reduced matrix element and its sign (eq 3) determines the sign of the mixing coefficient.[26] Often the sign of the direct matrix element is identical to that of the reduced one, but sometimes the sign of the reduced matrix element is opposite to the that of direct matrix element. This occurs especially when the direct matrix element is small and the reduced matrix element is dominated by the positive $-E_iS_{ss}$ term (eq 3) that overshadows the small negative hoping term. This is well apparent by inspection of the VBSCF and BOVB outputs. The positive reduced matrix element is interpreted formally as an effect of improving the Coulomb correlation in the fundamental structure. For an in-depth discussion of such cases, see: Shurki, A.; Hiberty, P. C.; Shaik, S. *J. Am. Chem. Soc.* **1999**, *121*, 822.

(29) Yu, M.; Dolg, M.; Fulde, P.; Stoll, H. *Int. J. Quantum Chem*. **1998**, *67*, 157.

bonding. Alternatively,[30b] a wave function made only from $^3\Phi_{ss}$ and $^3\Phi_{zz}$ can be rewritten as a wave function in which the electrons reside in two orbitals in mismatch, one hybridized inward and the other outward and vice versa. In this second sense, the mixing of $^3\Phi_{zz}$ into the fundamental configuration enables the electrons to get away from each other and lower thereby their triplet repulsion. The fundamental significance of no-pair bonding is thus quite apparent.

No-Pair Bonding in $^{n+1}Li_n$ Clusters. The VB model for no-pair bonding enables some qualitative insight into the high-spin clusters $^{n+1}Li_n$ in Table 1. Thus, since the major structure is the all s-configuration, $^{n+1}\Phi_{s\ldots s}$ (all electrons reside in AO-hybrids having a dominant 2s character), the preferred geometry of the cluster will tend to be one which minimizes the triplet repulsion. The total triplet repulsion is a sum of pair repulsions, and since the pair repulsion rises steeply as the Li−Li distance decreases, it is easily shown the lowest triplet repulsion will be maintained *in a geometry with uniform Li−Li distances*. The clusters in Table 1 have virtually uniform distances.

Since the resonance energy that leads to no-pair bonding is cumulative, summed over the secondary VB structures of the σ-type, the bond energy can be expressed as a function of the cluster size (n) as follows:

$$D_{\text{no-pair}}(^{n+1}\text{Li}_n) = -\sum_i \delta\epsilon_{\text{mix},i} - 0.5\delta E_{\text{rep}}(\text{Li-Li})\sum_{j=1}^{n} C_j \quad (6)$$

The first term sums up the individual VB mixing terms, $\delta\epsilon_{\text{mix},i}$ due to the secondary VB structures (excluding the fundamental one), indexed as Φ_i. The second term sums all the pairwise close neighbor triplet repulsions, where C_j is the coordination number of the jth atom in the cluster. Since each pair of interacting atoms in the cluster generates a few VB structures, the VB mixing term will increase initially more steeply as a function of the coordination number of the atom, in comparison with the triplet-repulsion term. It is apparent then that, to maximize the number of contributing VB structures and optimize thereby the resonance energy due to VB mixing, the no-pair clusters will prefer a geometry that maximizes the coordination number of the atom. It follows therefore that *the no-pair clusters will assume geometries which maintain uniform Li−Li distances and afford a maximal coordination number for the constituent atoms*. This conclusion is in accord with the findings in Table 1.

To utilize the equation in a semiquantitative manner, we make some simplifying assumptions: First, the $\delta\epsilon_{\text{mix}}$ and δE_{rep}(Li−Li) terms can be treated as average constant quantities that can be taken from the Li_2 study.[30c] Second, the contributing configurations are the monoionic and the nonredundant covalent types. By analogy to the $^3\Phi_{ss}$ and $^3\Phi_{zz}$ configurations in the Li_2 case, the covalent structures which are considered are the σ-types, $^{n+1}\Phi_{s\ldots s}$ and $^{n+1}\Phi_{p\ldots p}$, with occupations in hybrids which involve major 2s and 2p characters, respectively. Third, the monoionic structures are limited to those where the charges reside on close neighbors. On the basis of these assumptions, the number (m) of configurations becomes

$$m_{\text{cov}} = m_{\text{AO}} \quad m_{\text{AO}} = 3, \text{ for } ^{n+1}\text{Li}_n,\ n \geq 3 \quad (7a)$$

$$m_{\text{ion}} = 0.5 m_{\text{AO}}(m_{\text{AO}} - 1)\sum_j C_j \quad (7b)$$

$$m_{\text{tot}} = 3 + 3\sum_j C_j \quad n \geq 3\ (m_{\text{tot}} = 4 \text{ for } \text{Li}_2) \quad (7c)$$

where m_{AO} is the number of AO's used for Li atom to bind the cluster. If one retains for each atomic vertex only the 2s and the two tangential 2p hybrid orbitals while one excludes the 2p orbital perpendicular to the cluster's surface (the π-bonder AO), the number of hybrid AO's contributing to the skeletal bonding of the cluster is $m_{\text{AO}} = 3$ (unless we are dealing with Li_2 for which $m_{\text{AO}} = 2$). The total number of contributing VB structures for a cluster with $n \geq 3$ becomes then eq 7c. Having enumerated the contributing VB structures, we can estimate the no-pair bond energy as follows:

$$D_{\text{no-pair}}(^3\text{Li}_2) = -3\delta\epsilon_{\text{mix}} - \delta E_{\text{rep}} \quad (8a)$$

$$D_{\text{no-pair}}(^{n+1}\text{Li}_n) = -(3 + 3\sum_j C_j)\delta\epsilon_{\text{mix}} - 0.5\delta E_{\text{rep}}\sum_j C_j \quad n \geq 3 \quad (8b)$$

One can show that the expression behaves physically correct, and at an infinite cluster size the no-pair bonding energy per Li atom converges to a finite constant quantity (given by $[3\delta\epsilon_{\text{mix}} - 0.5\delta E_{\text{rep}}]C$, where C is the common coordination number in the cluster). Using eq 8, and the average $\delta\epsilon_{\text{mix}}$ and δE_{rep} quantities extracted from the dimer,[30c] we calculated no-pair bonding energies of 0.0278, 0.4554, 0.8178, 1.0596, and 1.5427 eV for the $^{n+1}Li_n$ cluster, $n = 2-6$. The results, which are in reasonable qualitative agreement with Table 1, *indicate that no-pair bonding is sustained by a cumulative resonance energy (due to VB mixing) which competes against the repulsion of the high-spin electrons*. The model equation, albeit crude, based on the VB bonding mechanism of the dimer seems to capture the chemical behavior of the no-pair bonded clusters. It is apparent that *this bonding form is fundamental and potentially of significant strength for sustaining large magnetic clusters*. Its experimental characterization is therefore challenging from both practical and intellectual points of view.

5. Conclusion

We asked at the outset the following: "what are the origins of no-pair bonding?" Our VB calculations (VBSCF and BOVB) provide a bonding mechanism which answers the question. The source of bonding of the no-pair bond appears to be similar to the single-pair bond in the sense that both are essentially covalent bonds, augmented by valence and dynamic electron correlation. However, while the covalent structure ($^1\Phi_{ss}$, Figure 4) of the singlet pair in the ground state of Li_2 is bonded, the corresponding triplet covalent structure ($^3\Phi_{ss}$, Figure 1) is repulsive and *the no-pair bonding arises from the delocalization due to resonance mixing of the secondary VB structures (Figure 5b,c)*.

(30) (a) According to the mixing rules in ref 26, $\langle|s_a s_b||\mathbf{H}||z_a z_b|\rangle = -2\beta_{ab}S_{ab}$, where β_{ab} is the reduced resonance integral between s_a and z_b (or z_a and s_b) and S_{ab} the corresponding overlap integral. This is analogous to the covalent energy of a singlet structure. (b) A wave function made of the two configurations, $\Psi = |s_a s_b| + \delta|z_a z_b|$, can be rewritten as $\Psi = |(s_a + \lambda z_a)(s_b + \lambda z_b)| + |(s_a - \lambda z_a)(s_b - \lambda z_b)|$; $\lambda^2 = \delta$. Any one determinant in the right-hand expression involves two electrons occupying orbitals in mismatch; one is hybridized slightly outward the other inward, and the roles (outward−inward) are reversed in the second determinant. (c) The repulsion energy of the fundamental configuration is determined (based on BOVB/cc-pVDZ results) as 1.504 kcal/mol (0.06522 eV) from the variationally optimized $^3\Phi_{ss}$ relative to the separated Li atoms. The difference between the no-pair bonding energy and this quantity is taken as the ΔE_{mix} term in Figure 5b (2.145 kcal/mol (0.093 eV)). To obtain an average effective $\delta\epsilon_{\text{mix}}$ quantity, we neglect the less important π type structures and remain then with three secondary configurations: two ionic, $^3\Phi_{sz}$(ion), and one covalent, $^3\Phi_{zz}$. The ΔE_{mix} is then divided by 3 yielding $\delta\epsilon_{\text{mix}} = 0.7143$ kcal/mol (0.031 eV), which is used in eq 8.

The resonance stabilization of the no-pair bond due to VB mixing is cumulative, summed over the contributing VB structures. This behavior enables one to extend the model to larger high-spin clusters $^{n+1}Li_n$. Thus, the highly symmetric geometry of the clusters originates in the preference of the fundamental high-spin configuration $^{n+1}\Phi_{s...s}$ for uniform bonds which thereby minimize the triplet repulsion. The increase of bonding with the cluster size arises due to the increase of the number of VB structures which contribute to the delocalization energy by VB mixing with $^{n+1}\Phi_{s...s}$. This resonance energy increases with the coordination number of the atom in the cluster, and since the resonance energy dominates the repulsion energy, the most stable no-pair clusters will assume the maximal possible coordination number. Characterization of larger no-pair clusters will bring much required novelty to the science of chemical bonding.

Acknowledgment. We are grateful to J. H. van Lenthe and C. P. Byrman for making TURTLE available. This research is supported by the ISF established by the Israeli Academy of Sciences and Humanities. This paper is dedicated to Lionel Goodman on the occasion of his 70th birthday.

JA982913N